Cement and Concrete Research 40 (2010) 1704–1713

Contents lists available at ScienceDirect

Cement and Concrete Research

journal homepage: http://ees.elsevier.com/CEMCON/default.asp

Early age hydration and pozzolanic reaction in natural zeolite blended cements: Reaction kinetics and products by *in situ* synchrotron X-ray powder diffraction

R. Snellings [a,*], G. Mertens [a], Ö. Cizer [b], J. Elsen [a]

[a] Department of Earth and Environmental Sciences, Katholieke Universiteit Leuven, Celestijnenlaan 200E, B-3001 Heverlee, Belgium
[b] Department of Civil Engineering, Katholieke Universiteit Leuven, Kasteelpark Arenberg 40, B-3001 Heverlee, Belgium

ARTICLE INFO

Article history:
Received 1 April 2010
Accepted 17 August 2010

Keywords:
Zeolite
Blended cement (D)
Hydration (A)
Kinetics (A)
X-ray diffraction (B)

ABSTRACT

The *in situ* early-age hydration and pozzolanic reaction in cements blended with natural zeolites were investigated by time-resolved synchrotron X-ray powder diffraction with Rietveld quantitative phase analysis. Chabazite and Na-, K-, and Ca-exchanged clinoptilolite materials were mixed with Portland cement in a 3:7 weight ratio and hydrated *in situ* at 40 °C.

The evolution of phase contents showed that the addition of natural zeolites accelerates the onset of C_3S hydration and precipitation of CH and AFt. Kinetic analysis of the consumption of C_3S indicates that the enveloping C–S–H layer is thinner and/or less dense in the presence of alkali-exchanged clinoptilolite pozzolans. The zeolite pozzolanic activity is interpreted to depend on the zeolite exchangeable cation content and on the crystallinity. The addition of natural zeolites alters the structural evolution of the C–S–H product. Longer silicate chains and a lower C/S ratio are deduced from the evolution of the C–S–H *b*-cell parameter.

1. Introduction

The contemporary cement industry has faced with the challenge of producing more sustainable, less energy intensive and more durable products without sacrificing the mechanical properties of the end product. One of the most widespread developments with limited interference in the conventional production process is the blending of supplementary cementitious materials or pozzolans with Ordinary Portland Cement (OPC) [1]. The replacement of a specific amount of cement clinker with pozzolans results in a proportional decrease in the economic and environmental cost of the end product. Moreover, the use of pozzolans in blended cement and concrete applications has been observed to significantly improve the cement durability, especially the vulnerability to chemical attack or alkali-aggregate reaction can be mitigated [2].

The broad group of pozzolanic materials consists mainly of (alumino-)silicate materials which share the ability to combine with portlandite ($Ca(OH)_2$) in the presence of water to form reaction products with binding properties in a process designated as the pozzolanic reaction [3]. Among these materials are industrial by-products such as slags, fly-ashes and microsilica, but also naturally occurring materials such as vitreous pumice, diatomite earths and zeolitised tuffs [2]. Zeolite tuffs are the diagenetically altered counterparts of vitreous pumice and occur in abundant quantities in areas of recent or ancient volcanism. As the deposited volcano-sedimentary sequences have frequently experienced diagenetic zeolitisation, zeolite tuffs represent probably one of the most abundant natural sources of pozzolanic material [4]. Zeolites belong to the tectosilicate mineral group and are build up by a framework of corner-sharing (alumino-)silicate tetrahedra. The framework is arranged as such to form a microporous structure with large cages (diameters of less than 2 nm) connected into channels. The resulting voids are occupied by water molecules and metal cations to compensate for the substitution of Si^{4+} by Al^{3+} in the framework. The extra-framework species are weakly bound to the framework and are exchangeable. The zeolite crystals occurring in diagenetically altered tuffs are generally very fine-grained (crystal size typically 10–100 μm) and show important concentrations of crystal defects. In contrary, hydrothermally precipitated zeolite crystals occurring in vugs and geodes can grow up to cm-sizes and possess few defects.

The reactivity of pozzolans or pozzolan activity is generally conceived as the rate of the pozzolanic reaction and is usually measured in terms of the evolution of the portlandite weight fraction or of the Ca^{2+} concentration in the pore solution over time [3,5]. Natural zeolite tuffs have shown to be more reactive than chemically similar unaltered vitreous pumice or tephra [6]. Moreover, zeolite tuffs presented a superior pozzolanic activity over many widely used industrial by-products such as fly-ashes and blast-furnace slags [7–9]. Especially the higher specific surface area available for reaction and the open zeolite structure have been suggested to contribute increased reactivity [6,10,11]. In addition to these factors, the absolute zeolite content of the pozzolanic material and the zeolite crystal chemistry, i.e. the framework Si/Al ratio and the exchangeable cation content, were observed to influence both long and short-term reactivity, respectively. Zeolites with an elevated Si/Al ratio showed higher long-term pozzolan

* Corresponding author. Tel.: +32 16 327593; fax: +32 16 326401.
E-mail address: ruben.snellings@ees.kuleuven.be (R. Snellings).

0008-8846/$ – see front matter © 2010 Elsevier Ltd. All rights reserved.
doi:10.1016/j.cemconres.2010.08.012

activities and better mechanical properties compared to low silica zeolites [11–13]. Zeolite tuffs containing exchangeable alkali cations changed the cement pore solution chemistry and increased the rate of pozzolanic reaction with respect to zeolite tuffs having predominantly Ca^{2+} as exchangeable cation [11,14–16]. A first *in situ* synchrotron radiation X-ray powder diffraction (SR-XRPD) study on the pozzolanic reaction between zeolite tuffs and portlandite [14] has pointed out that the reaction kinetics and the structural evolution of the main C–S–H reaction product (cement chemistry notation: C = CaO, S = SiO_2, H = H_2O, A = Al_2O_3; F = Fe_2O_3, and $\hat{S}$ = SO_3) were influenced by the exchangeable cation content.

In contrast to the limited number of SR-XRPD studies on the pozzolanic reaction *in se*, the advantages of SR-XRPD have been exploited more frequently to study the *in situ* hydration processes of single or mixtures of cement components [17–19], in Portland cements [19–22] and in belite cement systems [23,24] with or without additives or at various temperatures. The superior intensities and resolution of synchrotron radiation compared to laboratory X-ray sources in combination with the advent of powerful new detector systems allow to follow *in situ* reactions with an increased time resolution. Rietveld quantitative phase analysis of the recorded patterns allows to quantitatively analyse the consumption of starting materials and formation of crystalline reaction products. In addition, crystal structural parameters evolving during the reaction can be followed [14,18].

In this paper, the hydration of natural zeolite blended cements at 40 °C was investigated by means of *in situ* SR-XRPD. The combined action of the Portland cement hydration reactions and the pozzolanic reaction of the added natural zeolites was quantitatively determined by kinetic analysis of the Rietveld quantitative phase analysis results. To examine the influence of zeolite type on the cement hydration kinetics, two different types of zeolite materials were used: a well-crystallized hydrothermal Ca-rich chabazite (general structure formula $Ca_2Al_4Si_8O_{24}.12H_2O$; Si/Al = 2), representing natural zeolites of high crystallinity with low Si/Al ratio, and a diagenetically zeolitised tuff predominantly composed of clinoptilolite (general structure formula $(Na,K,Ca_{0.5})_7Al_7Si_{29}O_{72}.22H_2O$; Si/Al = 4.1), representing more siliceous zeolites of typically lower crystallinity. In order to assess the impact of zeolite crystal chemistry on the hydration processes, the clinoptilolite tuff was exchanged to its Na-, K-, and Ca-forms, each added as supplementary cementitious material.

2. Experimental

2.1. Material preparation and characterization

The OPC used was a commercial cement classified as CEMI 52.5R. Zeolite blended cements were prepared with a 3:7 zeolite:cement weight ratio. This ratio allows to investigate the consumption and structural evolution of the pozzolan more easily than lower replacement ratios. In practice optimal cement replacement ratios around 10–20 wt.% are more frequently reported [25–28], but higher replacement ratios from 30 up to 55 wt.% have also been found suitable for application [29–31]. The selected clinoptilolite tuff originated from Buckhorn, New Mexico (USA), and the chosen chabazite sample was a well-crystallized specimen from Wasson's Bluff, Nova Scotia (Canada). The samples were hand ground in an agate mortar to pass a 250 μm sieve and were subsequently wet milled in a McCrone Micronising Mill® with methanol. Wet grinding has been shown to result in a narrow Gaussian grain size distribution. After wet milling the granulometry was determined by laser diffractometry on a Malvern Mastersizer S Long Bed with a 300RF optical lens. Final mean grain size diameters (d_{50}) were 7.4 and 9.1 μm for the clinoptilolite and the chabazite material respectively. Cation exchange of the ground clinoptilolite tuff was performed by immersing the samples in nearly saturated NaCl, KCl and $CaCl_2$ solutions. The solutions were stored in closed containers at 60 °C to enhance the exchange process. After 1, 3, 5, and 10 days the solutions were renewed. The cation concentrations in the outcoming solutions were monitored by Atomic Absorption Spectroscopy (AAS) to determine the rate of cation exchange. After 14 days, the cation exchange was considered to be complete and the samples were separated from the solution by centrifugation and triply washed with distilled water to remove remainders of soluble salts.

The bulk chemical composition of the starting materials was analysed by Inductively Coupled Plasma Optical Emission Spectroscopy (ICP-OES), and an anhydrous lithium metaborate fusion flux was used to dissolve the samples. SO_3 content was indirectly derived from the Rietveld quantification results of gypsum and anhydrite. Loss on ignition (LOI) was determined by heating the samples for 2 h at 1050 °C.

The mineralogical phase composition of the starting materials was analysed by SR-XRPD using Rietveld analysis. A 10 wt.% ZnO spike was thoroughly intermixed with the samples to allow the calculation of the amorphous phase content. The samples were subsequently loaded into 2 mm capillaries and SR-XRPD patterns were collected at the BM01b beam line of the European Synchrotron Radiation Facility in Grenoble (France). The wavelength used was 0.50199 Å, calibrated to the NIST SRM 640b Si standard. The measurements were recorded in transmission geometry over an angular range of 1–26.5° 2θ, with a step size of 0.003° 2θ and a scan time of 200 ms per step. The phase quantification procedure initiated with the identification of major and minor mineral phases by the DiffracPlus EVA software (Bruker) and proceeded with full-profile Rietveld quantitative phase analysis (QPA) using the Topas Academic v4.1 software [32]. Peak profiles were fitted using the fundamental parameters approach [33]. The initial crystal structure information of the identified phases was adopted from the

Table 1
Chemical and mineralogical phase composition of the cement and zeolite starting materials. The designation 'other' comprises mainly X-ray amorphous phases and possibly some crystalline phases present in minor or trace amounts.

Portland cement (CEMI52.5R)				Clinoptilolite tuff						Ca-chabazite			
Chemistry	wt.%	Mineralogy	wt.%	Chemistry	Ca-clinoptilolite wt.%	K-clinoptilolite wt.%	Na-clinoptilolite wt.%	Mineralogy	wt.%	Chemistry	wt.%	Mineralogy	wt.%
SiO_2	20.58	C3S [34]	65.7	SiO_2	63.74	62.73	63.29	Clinoptilolite [14]	90	SiO_2	52.55	Chabazite [43]	91.6
Al_2O_3	4.67	β-C2S [35]	6.5	Al_2O_3	12.03	11.79	11.94	Quartz [41]	1	Al_2O_3	15.7	Quartz [41]	7.9
Na_2O	0.44	α′L-C2S [36]	0.5	Na_2O	0.41	0.34	6.57	Plagioclase [42]	1.6	Na_2O	0.81		
CaO	63.01	C3A [37]	5.7	CaO	5.41	0.1	0.13			CaO	7.47		
K_2O	0.62	C4AF [38]	8.2	K_2O	0.91	10.36	0.86			K_2O	0.68		
MgO	1.85	$C\hat{S}$ [39]	2.7	MgO	1.14	0.59	0.65			MgO	0.08		
TiO_2	0.45	$C\hat{S}H2$ [40]	0.6	TiO_2	0.16	0.16	0.16			TiO_2	0.01		
Fe_2O_3	3.79	Quartz [41]	0.1	Fe_2O_3	1.45	1.42	1.36			Fe_2O_3	0.05		
P_2O_5	0.76			P_2O_5	0.17	0.17	0.03			P_2O_5	0.16		
SO_3	2.12												
LOI	1.31	SUM	89.9	LOI	14.96	12.55	13.65	SUM	92.6	LOI	20.85	SUM	99.5
SUM	99.6	Other	10.1	SUM	100.37	100.21	98.63	Other	7.4	SUM	98.35	Other	0.5

literature. Table 1 lists the references for all crystal structures used together with the analysed chemical and mineralogical composition. The refinement procedure consisted of the fitting of the zero error, phase specific scale factors, unit cell parameters and Lorentzian peak shape broadening (CS_L) parameters. The background was fitted to a cosine Chebyschev function of 15 polynomial terms.

2.2. Synchrotron XRPD data collection and analysis

To study the interaction of zeolites and hydrating Portland cement, the zeolite blended cement pastes and a reference cement paste were monitored by SR-XRPD during hydration. The cement samples were thoroughly mixed with distilled water in a 0.6 water:cement ratio and transferred immediately to 2 mm diameter SiO_2 capillaries. The capillaries were subsequently sealed with epoxy glue and fixed on goniometer heads for measurement. The interference of the SiO_2 capillaries in the cement hydration is considered to be negligible during the early reaction up to 28 days because finely ground quartz present in the chabazite sample was left largely unreacted over this time span. The first SR-XRPD measurement started 10 min after the addition of water and the recording conditions were identical to the conditions used for the starting material characterization except for the scan time per step which was lowered to 100 ms. Under these conditions the duration of one scan was about 12.5 min. To accelerate the hydration reactions the samples were heated during measurement to 40 °C with a hot air blower. Uninterrupted monitoring by time-resolved SR-XRPD was continued up to 8 h of hydration; from then on the samples were stored at 40 °C and measured at specific time intervals to extend the period of data collection up to 3 days. In addition, separate identical samples were prepared at 7, 11, 14, 18, and 28 days in advance and stored at 40 °C to allow the extrapolation of the results up to ages typical for standard cement testing.

The Rietveld analysis of the time-resolved measurements involved the fitting of global parameters and phase specific scale factors, the initially refined structure models of the starting material components were fixed. However, unit cell and peak shape broadening parameters were refined for the zeolite and for the hydrated reaction product phases as both showed distinctive trends in structural evolution. The structure models for the crystalline reaction products were adopted from literature (portlandite or CH [44], ettringite (AFt) or $C_6A\hat{S}_3H_{32}$ [45], kuzelite (AFm) or $C_4A\hat{S}H_{12}$ [46]). The appearance and the intensity increase of broad reflection peaks at *d*-values of 3.06, 2.80, 1.82 and 1.67 Å showed the formation of the C–S–H as the primary cement hydration product. The structural evolution of this weakly crystalline phase was followed by introducing a "peaks phase" which allowed to fit and to investigate the evolution of the reflection positions, intensities and widths. As an example, the Rietveld fitted pattern of the K-exchanged zeolite blended cement after 6 h of hydration is shown in Fig. 1.

Rietveld-based methods for quantitative phase analysis require the calculation of a phase constant which relates the refined scale factor S_i of phase i to the respective weight fraction W_i according to the following relationship (Eq. (1)) [47],

$$W_i = \frac{(ZMV)_i S_i}{\sum_n (ZMV)_n S_n} \quad (1)$$

where Z identifies with the number of formula units in the unit cell, M with the unit cell mass and V with the unit cell volume. It should be remarked that the sum of the weight fractions of all crystalline phases is normalized to 1 in Eq. (1). However, the addition of an internal standard to the dry mixes allowed the calculation of the amorphous phase content [48]. During hydration of the cements the main C–S–H reaction product is initially heterogeneous and is not showing well-developed long-range order, in consequence it cannot be directly quantified. Therefore, instead of adding a substantial amount of internal standard which could influence the hydration process, the conversion of the refined scale factors to weight fractions was made under the assumption of constant sample scattering mass through time. In that case, the total scattered intensity through time can be considered constant and weight fractions can be obtained by multiplying the phase fractions with a phase specific constant [22]. However, in order to obtain absolute weight fractions the initially determined amorphous weight fraction and the difference in irradiated sample mass between the dry cement and the cement paste should be taken into account. The former can be easily introduced by multiplying the phase specific constants with the refined total weight fraction of crystalline phases, and the latter can be taken into account by dividing the phase specific constant by P which is the ratio of the scale factor of an initially unreactive phase in the first time-resolved measurement of the hydrating paste over the respective phase scale factor in the dry mixture. This ratio should be the same for all initially unreactive phases. In the zeolite-cement pastes several phases (C_3S, β-C_2S and C_4AF) qualify for the calculation of P because at the beginning of the acceleration period, this is generally 1 h after mixing, the total degree of hydration is typically only 0.1–1% [49]. In consequence, after 10 min of hydration, the expected differences in absolute cement component weight percentages between the dry mix and the paste are expected to be smaller than the typical standard deviation for Rietveld quantitative phase analysis [50]. The factor P is a

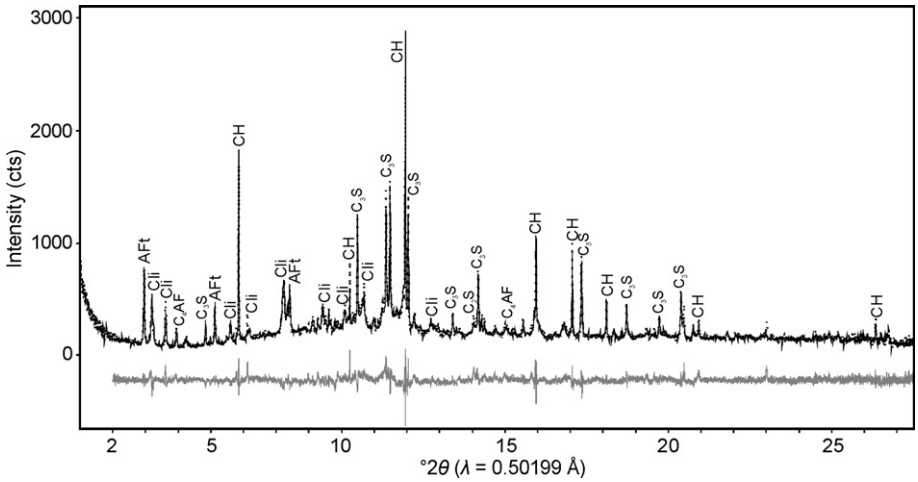

Fig. 1. SR-XRPD Rietveld plot for the K-exchanged clinoptilolite blended cement after 6.0 h of hydration. The dashed line represents the experimental pattern, the full line is the calculated pattern and the grey line below is the difference curve between the experimental and the calculated pattern. Reflection positions of the major phases are marked (Cli = K-clinoptilolite).

constant for each separate mixture, therefore it should be identical for all phases present within the mixture. The eventual phase specific conversion factor K_i can then be calculated as in Eq. (2) and is valid for both reactants as hydrated reaction products

$$W_i = \frac{(ZMV)_i S_i}{\left(\sum_n (ZMV)_n S_n\right)_{dry}^{P}} \left(1 - W_{amorphous}\right) = K_i S_i. \quad (2)$$

Finally, the refined weight fractions refer to the dry cement mixture and are normalized straightforwardly with respect to the water content of the paste. It should be noted that the refined scale factors have to be corrected for the synchrotron beam current decay.

2.3. Kinetic analysis

The hydration of C_3S mainly controls the setting and the early strength development in Portland cement pastes [49]. The rate of hydration of C_3S can therefore be used to discriminate between the principal Portland cement hydration stages of induction, acceleration and deceleration. The reaction rate is usually expressed as the derivative of the fractional reaction α over time (Eq. (3)):

$$\frac{d\alpha}{dt} = kf(\alpha) \quad (3)$$

where k is the rate coefficient and the formulation of $f(\alpha)$ depends on the reaction mechanism. Plotting the reaction rate vs. α allows to distinguish the acceleration from the deceleration period. At the start of the deceleration period the controlling step in the C_3S hydration reaction mechanism is generally accepted to switch from the auto-catalytic growth of hydrated reaction products to the diffusion of dissolved reactant components through a barrier layer of reaction products [48]. To model the progress of the reaction over the deceleration period the modified Jander equation for three-dimensional diffusion processes is commonly used (Eq. (4)) [3,11,14,51]:

$$\left(1-(1-\alpha)^{1/3}\right)^N = K(t-t_0) \quad (4)$$

where t_0 identifies with the start of the deceleration period, K with the rate coefficient estimated by the Jander equation, and N with the reaction exponent which depends on the reaction mechanism. The rate limiting step of the reaction mechanism is surface dissolution or nucleation/precipitation if $N \leq 1$ and three-dimensional diffusion through a layer of reaction products if $N > 1$. The barrier layer of reaction products is assumed to grow or condense with increasing N-values. If $N \leq 2$ then the barrier layer is considered to be porous, if $N > 2$ then it is considered to be dense.

3. Results and discussion

The quantitative phase analysis of the Portland cement used in the experiments has indicated that C_3S is the main component; α'L- and β-C_2S are present in minor amounts typical for a CEMI class cement (Table 1). C_3A and C_4AF constitute the aluminate phases and most likely contain alkali impurities as inferred from bulk chemical analysis (Table 1). Mg can be partially accommodated in the C_3S phase [34]. A significant weight fraction (10.1 wt.%) of the cement was found to be composed of amorphous and possibly minor or trace amounts of other crystalline phases, which is consistent with data of De La Torre et al. [52] that report typical amorphous contents of the C_3S phase in OPC of 19 wt.%. The Ca-sulphates present as setting retarders were anhydrite and gypsum.

The zeolite tuffs contained high amounts (~90 wt.%) of chabazite and clinoptilolite, respectively. In the chabazite sample a minor amount of quartz was detected. Quantitative phase analysis indicated the presence of quartz, plagioclase feldspar and amorphous phase as accessory phases in the clinoptilolite tuff.

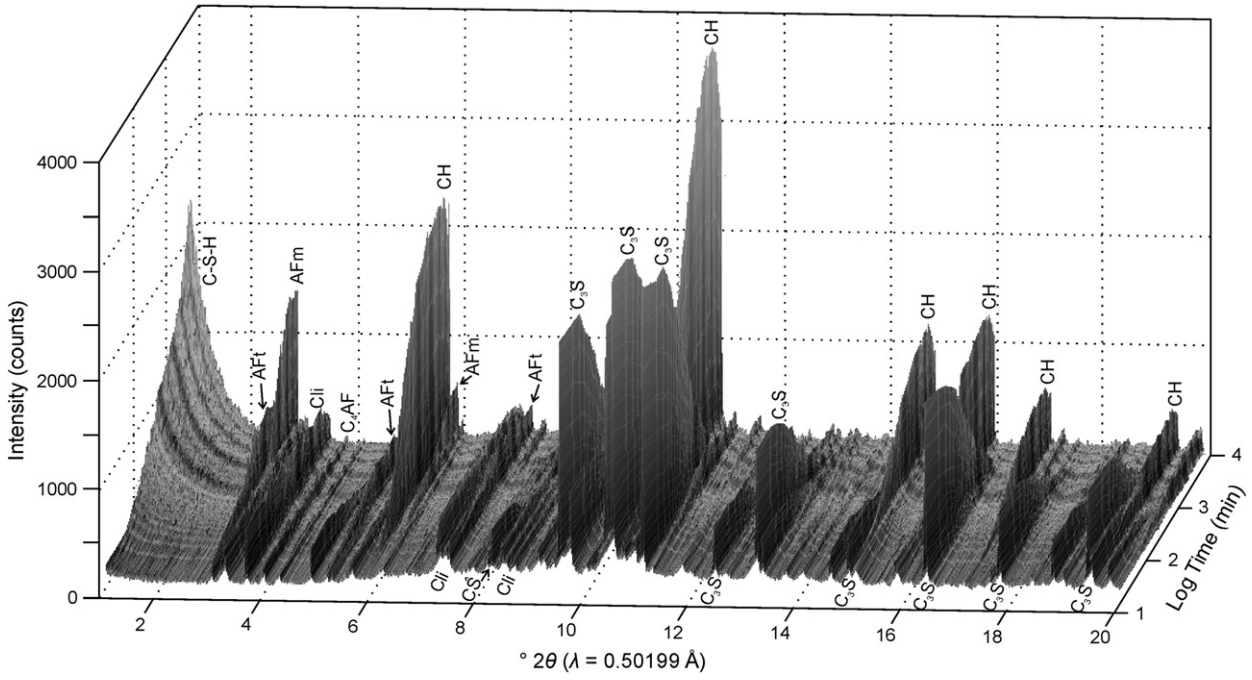

Fig. 2. Stack of synchrotron beam current decay corrected time-resolved SR-XRPD data for the K-exchanged clinoptilolite blended cement up to 4 days of hydration. The main reflection positions in the 1–20° 2θ region are indicated (Cli:K-clinoptilolite). The intensities of the anhydrous cement phases decreases sharply and the formation of crystalline (AFm, AFt and CH) and semi-crystalline (C–S–H) hydration products can be observed. The consumption of the K-clinoptilolite and CH in the pozzolanic reaction is noticeable towards the end of the displayed reaction period.

During the hydration of cement several reactions take place simultaneously or successively. The occurrence of one reaction can affect the kinetics and reaction products of a second reaction and so on, leading to a complex interplay of reactions. In Fig. 2 the evolution over time of the *in situ* SR-XRPD patterns of the hydrating K-clinoptilolite blended cement is reported. The AFt reaction product appeared immediately upon the addition of water to the system. The partial transformation of AFt into AFm usually occurs when no more sulphate is available to recombine. The C_3S and C_2S phases hydrate to form the C–S–H phase and CH. The consumption of the C_3S phase and crystallization of the CH phase are easily observed in Fig. 2. The appearance and growth of several broad peaks in the diffraction patterns around *d*-values of 3.06, 2.80, 1.82, and 1.67 Å indicate the formation of the C–S–H phase. In Portland cements blended with pozzolans the CH produced will react with the pozzolan to form additional C–S–H of lower C/S ratio and AFm phases [2,14]. The progress and kinetics of the series of hydration reactions presented above were investigated using Rietveld quantitative phase analysis. Fig. 3 illustrates the results for the hydrating reference Portland cement and the K-clinoptilolite blended cement system.

3.1. Hydration kinetics

The early hydration kinetics of the zeolite blended cements were compared to the hydration of the reference cement by modelling the hydration of the C_3S phase. C_3S is the major component of the mixes and its hydration behaviour is largely responsible for the setting and hardening of the pastes. In addition, C_3S reacts relatively rapidly when wetted. Therefore the C_3S hydration was considered to be the most suitable for the investigation of the early hydration kinetics of the zeolite blended cement pastes.

The hydration rate of C_3S in function of time is presented in Fig. 4 for all *in situ* hydrated samples. The evolution of the C_3S weight fraction in the reference cement showed that an induction period of low hydration rates is succeeded by an acceleration period of increasing reaction rates after approximately 100 min of hydration (cf. Fig. 3). A similar evolution was observed during the hydration of the chabazite blended cement, where slightly higher reaction rates were encountered during the induction period. In contrast, the addition of the natural clinoptilolite samples advances the onset of the acceleration period and greatly accelerates the C_3S hydration rate at early stages. Simultaneously, the consumption of C_3A and C_4AF is also enhanced. This acceleration seems to be largely independent from the type of exchanged cation. The advance of the onset

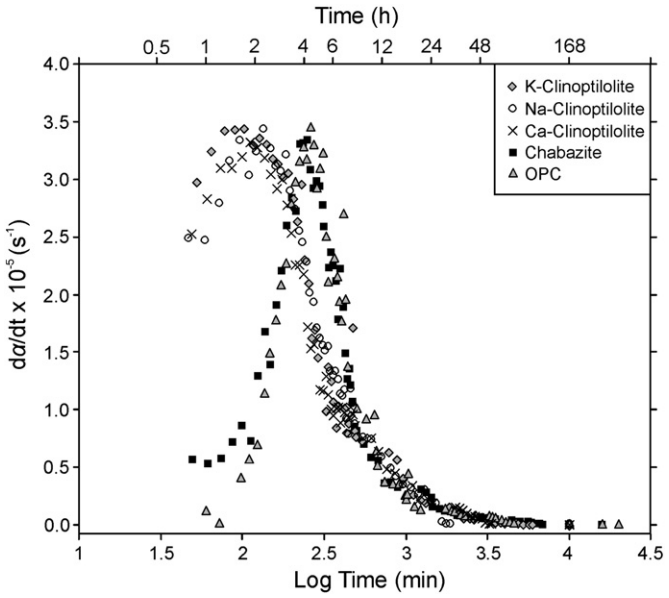

Fig. 4. Reaction rate of C_3S hydration vs. time. The hydration of C_3S initiated earlier in the clinoptilolite blended cements with respect to the reference OPC and the chabazite blended cement.

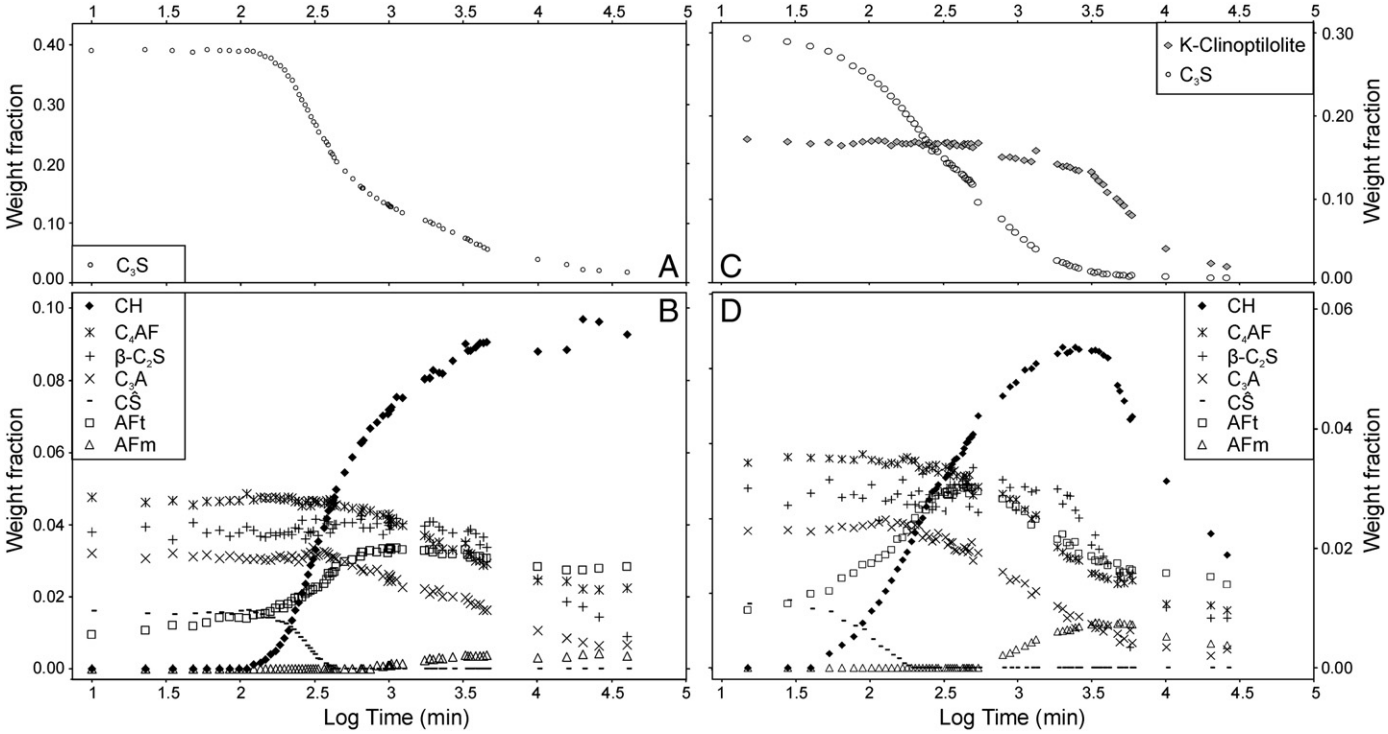

Fig. 3. The evolution of weight fractions determined by Rietveld quantitative phase analysis of the time-resolved SR-XRPD measurements on the hydrating reference cement paste (A and B) and on the hydrating K-clinoptilolite-cement paste (C and D). Note the differences in the vertical scales. The reported weight fractions refer to the cement pastes including the added water.

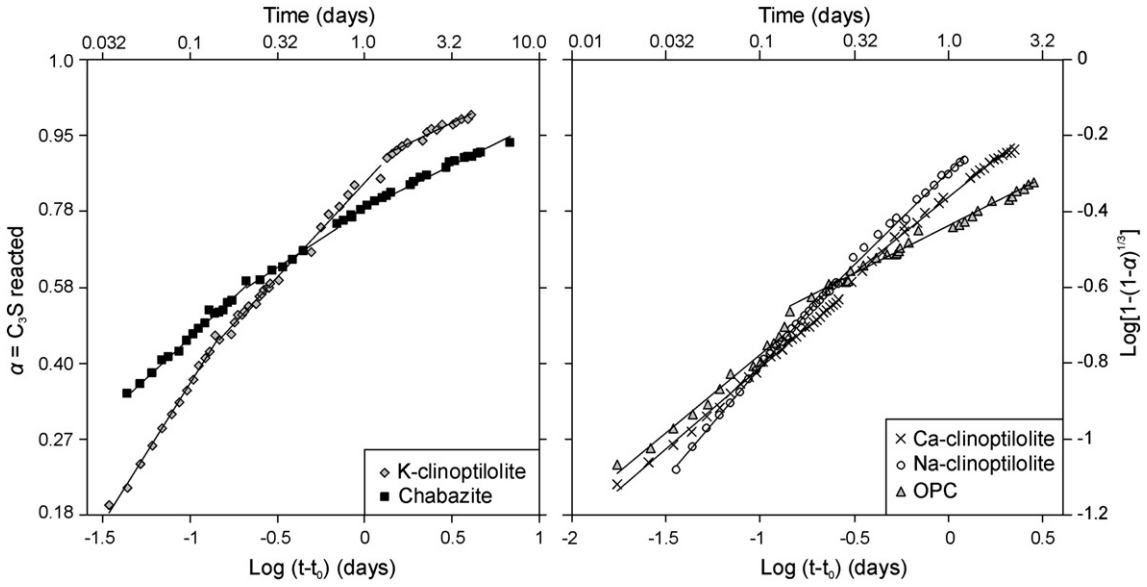

Fig. 5. Plots of modified Jander equation for the consumption of C_3S vs. $\log(t-t_0)$, expressed in days, the slope of the regression curves provides an estimation of the exponents of reaction *N*.

of the acceleration stage has also been reported from isothermal conduction calorimetry experiments and was related to the adsorption of Ca^{2+} on the pozzolan either as a surface layer or as C–S–H. This mechanism would allow the C_3S to dissolve more rapidly through a thinner or less dense layer of C–S–H growing on the C_3S grains [53]. The lower crystallinity of the clinoptilolite material with respect to the chabazite material probably allows an increased adsorption of Ca^{2+} and possibly explains the difference in C_3S hydration. It should be noted that the maximum C_3S hydration rate does not appear to vary over the different pastes.

The maximum hydration rates were reached in the clinoptilolite blended cements after approximately 2 h of hydration and after 4 h in the reference and chabazite blended cements. The deceleration of the hydration rate is generally considered to be caused by the thickening of the C–S–H barrier layer on the C_3S surface. The decreasing permeability of the barrier layer leads to a switch of the rate controlling reaction mechanism from a nucleation to a diffusion controlled process [49]. The modified Jander equation for three-dimensional diffusion processes was used as the kinetic model function for the hydration of C_3S during the deceleration period (Eq. (4)). The values of the reaction exponents *N* were determined from the slopes of the linear regression curves in a plot of $\log[(1-(1-\alpha)^{1/3})]$ vs. $\log(t-t_0)$, with time expressed in days to enable easy comparison with previous studies. The log–log plots for the hydration of C_3S in all investigated pastes are presented in Fig. 5. The values of the reaction exponents *N* over specified periods of time are reported in Table 2. The general increase over time of the *N*-values for all hydrating pastes is interpreted as a consequence of the continuous thickening and densification of the C–S–H barrier layer. However, the results present significant differences in *N*-values between the hydrating pastes analysed. It can be observed that at early stages of reaction, typically within the first 3 to 6 h of the deceleration period, the values of *N* are lower for the cement pastes blended with alkali-exchanged clinoptilolite. The *N*-values determined for the cements blended with clinoptilolite and chabazite with Ca^{2+} as predominant extra-framework cation are more similar to the *N*-value for C_3S hydration in OPC at 40 °C.

The ensuing period showed a divergence in reaction exponents. At this stage, according to the modified Jander equation, the barrier layer of C–S–H enveloping the C_3S grains is the thickest or the most dense in the OPC paste with a *N*-value of 4.00. In contrast, diffusion of dissolved species seems to be much less hampered by the C–S–H barrier layer in the blended cements. Especially in the alkali-exchanged clinoptilolite blended cements the C_3S surface layer is remarkably more permeable than in OPC, enabling a higher rate of C_3S hydration. This is corroborated by the fractional reaction α of C_3S after 24 h of hydration (Table 2). The value of α (C_3S) reaches 85 to 87% in alkali-clinoptilolite blends compared to 74% in OPC. The enhanced hydration rate of C_3S in the alkali-clinoptilolite blends can be related to the ability of zeolites to alter the pore fluid chemistry considerably [11,16]. The release of exchangeable alkali cations into solution suppresses the Ca^{2+} concentration through the common ion effect and influences the onset of portlandite precipitation [16]. Higher alkali and lower Ca^{2+} concentrations have been reported to lower the C/S ratio and alter the microtexture of the C–S–H reaction products [53]. Richardson [53] concluded from TEM observations that C–S–H reaction products with reduced C/S ratio in blended cements and C–S–H formed in cement pastes activated with KOH or NaOH show foil-like two-dimensional rather than fibrillar, one-dimensional morphologies. Similar observations were made by Renaudin et al. [55] based on the Rietveld refinement of anisotropic peak broadening in XRD patterns of synthetic

Table 2
Reaction exponents *N* obtained from the modified Jander equation over specified periods of reaction and the fractional reaction α at 24 h for the hydration of C_3S and the consumption of the added pozzolanic material.

	N	Period	*N*	Period	*N*	Period	α (C_3S) at 24 h (%)	α (Pozz) at 24 h (%)
K-clinoptilolite	1.40 (3)	2–5 h	2.01 (5)	5–31 h	4.5 (2)	31–99 h	85	16
Na-clinoptilolite	1.714 (16)	2–6 h	2.05 (3)	6–31 h			87	19
Ca-clinoptilolite	2.35 (2)	2–8 h	2.51 (4)	8–56 h			81	16
Chabazite	2.35 (6)	4–9 h	3.3 (3)	9–21 h	4.49 (9)	21–115 h	77	4
OPC	2.43 (9)	4–7 h	4.00 (8)	7–72 h			74	

C–S–H. The reported variation in morphology of the C–S–H particles with C/S ratio can partially explain the changing permeability of the reaction layer.

3.2. Pozzolanic reaction

The start of the pozzolanic reaction is marked by the onset of zeolite and CH consumption. Fig. 3C and D illustrate the evolution of the calculated weight fractions of CH and K–clinoptilolite. This general behaviour was encountered in all investigated blended cements. The exact timing of the onset of the pozzolanic reaction cannot be easily determined because of the low initial reaction rate and the continuous hydration of clinker phases producing CH. After ±10 h of reaction the K-clinoptilolite weight fraction has decreased by more than two esd's (estimated standard deviations). Initially the pozzolanic reaction of K-clinoptilolite accelerated relatively slowly until at approximately 2–3 days of hydration the maximum rate was reached. Subsequently the pozzolanic reaction rate decreased (Fig. 3). In Table 2 the fractional reaction at 24 h of the consumption of the zeolite pozzolans in the pozzolanic reaction is reported. The amount of zeolite reacted is the highest in the clinoptilolite blended cements (16–19 wt.%), and only 4 wt.% of chabazite has reacted at 24 h of hydration. After 14 days of reaction 89% of the K-clinoptilolite, 88% of Na-clinoptilolite, 79 of the Ca-clinoptilolite and 45% of the chabazite were consumed. The relative fractional reactions obtained for the exchanged clinoptilolites compare very well to the fractional reactions reported for the pozzolanic reaction in pastes of exchanged clinoptilolite and CH analysed by *in situ* SR-XRPD with Rietveld QPA [14]. It was suggested in [14] that the alteration in pore fluid chemistry could also explain the higher reactivity of the alkali-exchanged clinoptilolites. The lower reactivity of the chabazite sample is probably due to the much higher crystallinity. Though the grain size distributions of both materials were similar, the initially refined CS_L value for the chabazite sample was 580±26 nm. Instead the clinoptilolite showed a much lower value of 66±2 nm. The CS_L parameter is a phase specific constant calculated by the Scherrer equation and provides at least a qualitative indication about the real volume weighted mean crystallite sizes. This observation emphasises the need for detailed characterisation of the pozzolanic products and the important control of the natural origin or the production process on the eventual pozzolanic activity.

The natural zeolites added to the Portland cement all showed a remarkable structural evolution during hydration and reaction. Fig. 6 reports the variations of the unit cell volumes of the exchanged clinoptilolites. Chabazite showed a similar behaviour. The unit cell volumes were observed to expand instantaneously upon the addition of water to the system. Zeolite cell parameters have been shown to be very sensitive to (de)hydration. The adsorption of water generally increases the unit cell volume [56]. However, variations in unit cell volume can also result from changes in the exchangeable cation content, and this is exemplified by the differences in unit cell volume of the Na-, K-, and Ca-exchanged clinoptilolites as presented in Fig. 6. Additionally, leaching or preferential consumption of framework constituents altering the framework Si/Al can also effectuate unit cell volume changes. It is therefore difficult to relate the variations in unit cell volume to a single cause. Nevertheless, the similar expansion in all samples suggests that comparable processes occur.

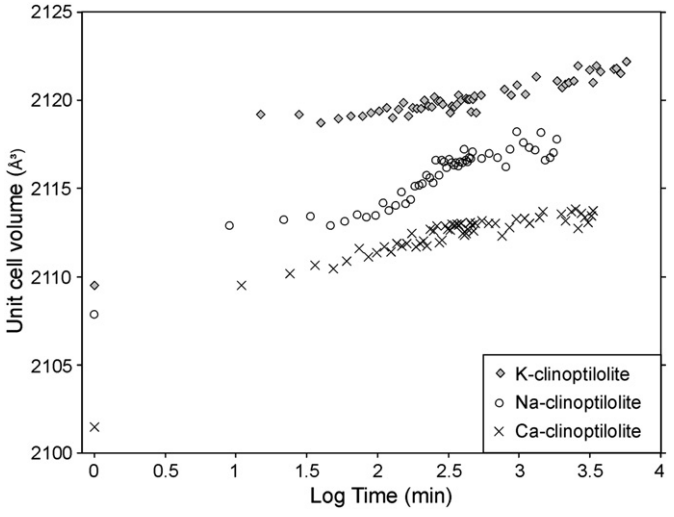

Fig. 6. Evolution of the unit cell volume of the exchanged clinoptilolites during reaction.

3.3. Reaction products

3.3.1. CH

The hydration of the clinker silicate phases, initially largely C_3S, resulted in the precipitation of crystalline CH and C–S–H. The advanced onset of C_3S hydration in the clinoptilolite-blended cements was simultaneous with the accelerated formation of CH. The CH precipitation rate followed the consumption rate of C_3S linearly over the first two days and CH weight fractions reached a maximum around 2–3 days of hydration (~3000 min), after which the pozzolanic reaction noticeably initiated the consumption of CH (Fig. 3C–D). In the reference cement, the crystalline CH weight fraction remained approximately constant at ±15 wt.% over the longer term up to 28 days of hydration (Fig. 3B). The maximum attained CH weight fractions in the zeolite blended cements are lower than the CH weight fraction in the reference cement multiplied by the cement dilution factor. In the chabazite blended cement, the CH weight fraction reaches no more than 92% of the expected value. The quantity of CH formed in the Portland cements blended with Na- and K-clinoptilolite amounts to 84% and in the Ca-clinoptilolite blended cement merely to 71% of the expected value. These observations can be partially explained by the adsorption of Ca^{2+} on the negatively charged pozzolan surface, the clinoptilolite offering more adsorption sites than the chabazite sample. Nevertheless, the reduction in the amount of CH could also result from the start of the pozzolanic reaction. In addition, the difference between the maximum attained CH fraction in the Ca-clinoptilolite blended cement with respect to alkali-exchanged clinoptilolite blended cements could be due to the common ion effect being much stronger in the latter pore fluids, forcing Ca^{2+} out of solution to precipitate as CH.

During precipitation the CH phase experiences an interesting structural evolution. The decrease in the *a*- and *c*-cell parameters as well as the evolution of the CS_L parameter is presented in Fig. 7. Similar structural trends were encountered in all samples. The shift or splitting of the (0 0 1) basal reflection has been reported recently, and suggested to be due to the presence of two different CH phases, one precipitated as crystalline CH from the pore solution and one as finely intercalated in the C–S–H structure [57]. Alternatively, the observed unit cell contraction can also be related to the 'healing' of structural defects during ongoing crystallization [58]. This is corroborated by the initially increasing CS_L parameter, implying the growth of the CH particles. At the onset of the pozzolanic reaction, however, the CS_L values of the CH start decreasing, pointing to a possible decomposition process during the consumption of CH.

3.3.2. AFt and AFm

Simultaneously with the advance of the onset of C_3S hydration in the clinoptilolite blended cements, the formation of AFt is accelerated with respect to the reference cement. The formation of AFm leads to a decrease in AFt content (Fig. 3B and D). The onset of the transformation reaction was observed to predate the start of the pozzolanic reaction and both seem to behave independently. Still, the formation of the AFm phase was more extensive in the blended cements. During hydration, also the AFt phase is undergoing

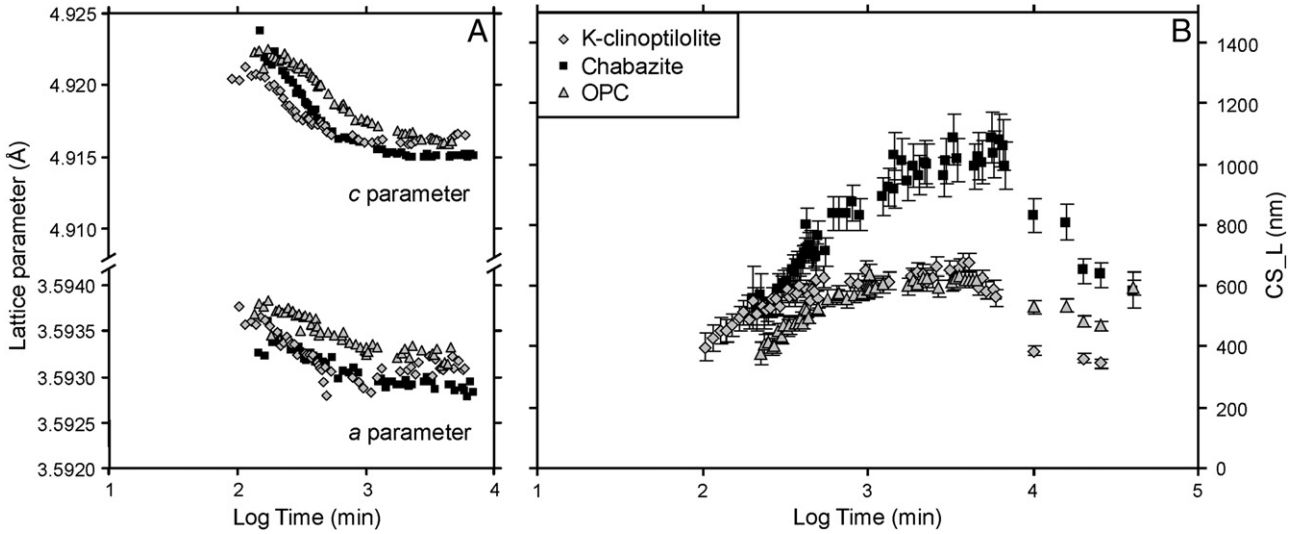

Fig. 7. The variation in CH lattice parameters (A) and CS_L parameter through time for the portlandite phase formed in the K-clinoptilolite and chabazite blended cements and the reference OPC.

structural changes. Besides a general increase in AFt crystallinity indicated by the increasing CS_L values, the *a*-cell parameter expanded and the *c*-parameter contracted substantially towards the ideal lattice parameters of pure ettringite over the course of 4–5 h (Fig. 8). Very similar AFt structural variations have been recently reported to occur during the early hydration of C_3A and gypsum [18] and of Portland cement [22,57,58]. The structural evolution of the AFt phase evidenced by *in situ* SR-XRPD, indicates that the AFt formation conditions, composition [18] and/or microstructural strain [59] evolve during hydration.

3.3.3. C–S–H

The formation of the C–S–H phase is marked by the appearance and by the intensity increase of broad peaks at *d*-values around 3.06, 2.80, 1.82, and 1.67 Å (Fig. 2). The refinement of the peak positions of the introduced 'peaks phase' demonstrated a considerable shift of the 1.82 Å peak to 1.83 Å over the course of reaction (Fig. 9). Recently, an orthorhombic *I2mm* super space group was put forward for the structure of C–S–H of varying C/S ratio [60]. In this model the 1.82 Å peak was indexed as the (0 2 0) reflection, directly related to C–S–H *b*-cell parameter. The *b*-axis is running parallel with the discontinuous 'dreierkette' chains of silicate tetrahedra attached to both sides of the Ca–O layer in the C–S–H structure. The length of the silicate chains increases with decreasing C–S–H C/S ratio as paired silicate tetrahedra become connected with a bridging tetrahedron to form pentamers, octamers, etc. Garbev et al. [60] reported that an increase of the C–S–H *b*-cell parameter was related to a lowered C/S ratio, and suggested that the insertion of bridging tetrahedra was responsible for the expanded *b*-parameter. In Fig. 9 the variation over time of the (0 2 0) reflection position is presented for the OPC and the chabazite and K-clinoptilolite blended cements. The increase of the *d*-value is much more marked in the blended cements compared to the OPC, pointing to the possible presence of a C–S–H phase with longer silicate chains and lower C/S ratio in the blended cements. This observation is in agreement with SEM/TEM and ^{29}Si NMR measurements of C/S ratios and silicate anion structure of the C–S–H phase in pozzolan blended cements [54].

4. Conclusions

Time-resolved SR-XRPD measurements combined with Rietveld quantitative phase analysis offer a powerful tool to elucidate the *in situ* hydration of zeolite blended Portland cements. Rietveld analysis has allowed to study the evolution of phase weight fractions,

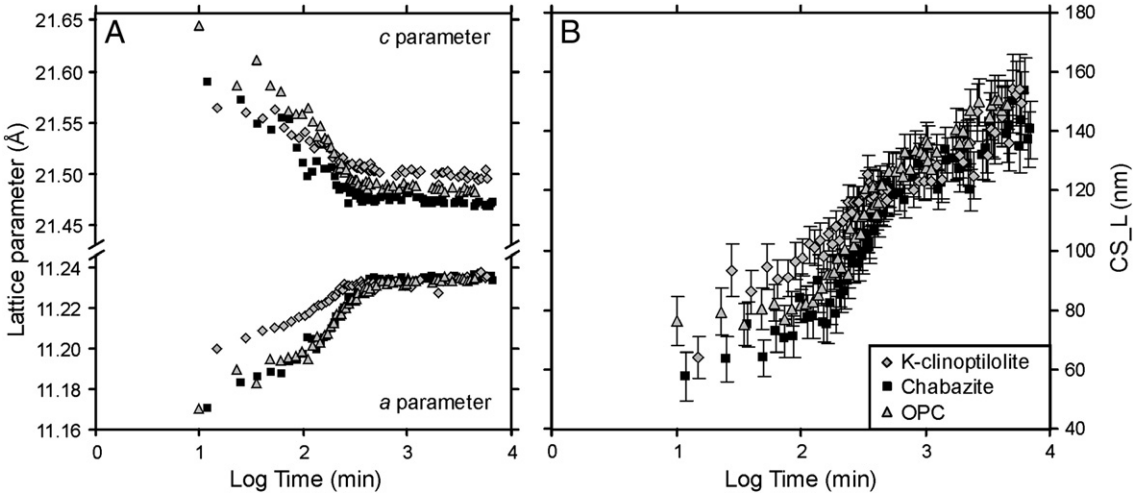

Fig. 8. The variation in AFt lattice parameters (A), and CS_L parameter through time for the AFt phase formed in the K-clinoptilolite and chabazite blended cements and the reference OPC (B).

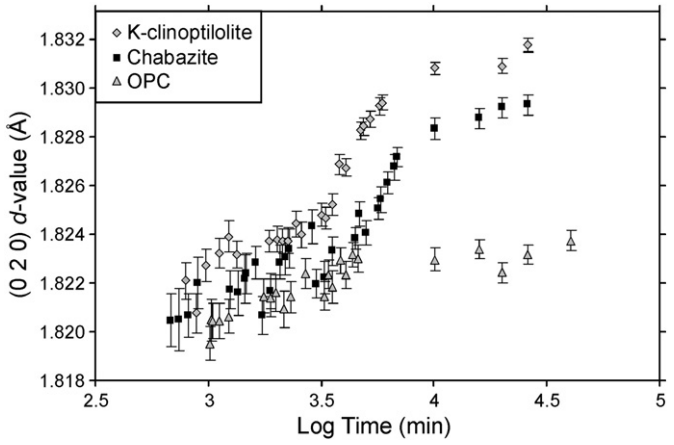

Fig. 9. Evolution of the C–S–H (0 2 0) reflection position during the hydration of the K-clinoptilolite and chabazite blended cements with respect to the variation observed in the reference OPC.

i.e. the consumption of anhydrous cement phases and zeolites and the neoformation of crystalline reaction products. In addition, structural variations of the reaction products and the zeolite reactants could be assessed.

The effects of the addition of natural zeolite pozzolans depend strongly on the zeolite characteristics. The onset of C_3S hydration, CH precipitation and AFt formation was substantially advanced by the addition of a natural clinoptilolite-rich tuff of low crystallinity. However, the inclusion of a chabazite sample, showing a similar grain size distribution but much higher crystallinity was much less effective in accelerating the setting of the cement. Moreover, the pozzolanic reaction rate was determined to be considerably lower for the well-crystallized sample.

An additional important zeolite property is the extra-framework cation content. The exchangeable cation content of the Na-, K-, and Ca-exchanged clinoptilolite tuff influenced the pozzolanic activity and the formation and diffusion characteristics of the C–S–H reaction products growing on the C_3S grains. The pozzolanic activity of alkali-exchanged clinoptilolites was higher than that of the Ca-exchanged clinoptilolite. The C–S–H phase structural evolution in the blended cements diverged from the C–S–H in the reference OPC. In the presence of zeolite pozzolans longer C–S–H silicate chains and lower C/S ratios were inferred from conspicuous shifts in reflection positions.

Acknowledgements

The constructive comments of two anonymous reviewers were highly appreciated. The authors acknowledge the European Synchrotron Radiation Facility for granting beam time. The skilful assistance of Herman Emerich at the Swiss-Norwegian beam line is gratefully acknowledged. Experimental material was kindly provided by Lieven Machiels. Elvira Vassilieva is thanked for assisting with the chemical analyses. The first author is currently working as aspirant for the Research Foundation - Flanders (FWO).

References

[1] J.S. Damtoft, J. Lukasik, D. Herfort, D. Sorrentino, E.M. Gartner, Sustainable development and climate change initiatives, Cem. Concr. Res. 38 (2) (2008) 115–127.
[2] F. Massazza, Properties and applications of natural pozzolanas, in: J. Bensted, P. Barnes (Eds.), Structure and Performance of Cements, 2nd edition, Spon Press, London, 2001, pp. 326–352.
[3] K. Takemoto, H. Uchikawa, Hydratation des ciments pouzzolaniques, Proceedings of the 7th International Conference on the Chemistry of Cement, Paris, France, 1980, IV–2, 1–29.
[4] C. Colella, M. de' Gennaro, R. Aiello, Use of zeolitic tuff in the building industry, in: D.L. Bish, D.W. Ming (Eds.), Natural Zeolites: Occurrence, Properties, Applications, Reviews in Mineralogy and Geochemistry, Mineralogical Society of America, Washington, 2001, pp. 551–588.
[5] D.J. Cook, Natural pozzolanas, in: R.N. Swamy (Ed.), Cement Replacement Materials, Surrey University Press, 1986, pp. 1–39.
[6] R. Sersale, Structure et caractérisation des pouzzolanes et des cendres volantes, Proceedings of the 7th Symposium on the Chemistry of Cement, Paris, France, 1980, IV–1, 3–21.
[7] S.Y.N. Chan, X. Ji, Comparative study of the initial surface absorption and chloride diffusion of high performance zeolite, silica fume and PFA concretes, Cem. Concr. Compos. 21 (1999) 293–300.
[8] C.S. Poon, L. Lam, S.C. Kou, Z.S. Lin, A study on the hydration rate of natural zeolite blended cement pastes, Construction Build Mater 13 (1999) 427–432.
[9] R.A. Gayoso Blanco, M.R. Lam, Non-conventional aggregates and mineral admixtures in high-performance concrete, ACI Special Publications 228 (2003) 123–134.
[10] B. Ligouri, D. Caputo, M. Marroccoli, C. Colella, Evaluation of zeolite-bearing tuffs as pozzolanic addition for blended cements, ACI Special Publications 221 (2003) 319–333.
[11] G. Mertens, R. Snellings, K. Van Balen, B. Bicer-Simsir, P. Verlooy, J. Elsen, Pozzolanic reactions of common natural zeolites and parameters affecting their reactivity, Cem. Concr. Res. 39 (2009) 233–240.
[12] G. Frigione, L. Bonavita, A. Katovic, G. Giordano, Synthetic zeolites as substitutes of silica fume, Proceedings of the 11th International Congress on the Chemistry of Cement, 2003, pp. 1325–1335.
[13] D. Caputo, B. Liguori, C. Colella, Some advances in understanding the pozzolanic activity of zeolites: the effect of zeolite structure, Cem. Concr. Compos. 30 (2008) 455–462.
[14] R. Snellings, G. Mertens, S. Hertsens, J. Elsen, The zeolite-lime pozzolanic reaction: reaction kinetics and products by *in situ* synchrotron X-ray powder diffraction, Microporous Mesoporous Mater. 126 (2009) 40–49.
[15] R. Snellings, G. Mertens, J. Elsen, Calorimetric evolution of the pozzolanic reaction of zeolites, J. Therm. Anal. Calorim. 101 (2010) 97–105.
[16] K. Luke, The effect of natural zeolites on the composition of cement pore fluids at early ages, Proceedings of the 12th International Congress on the Chemistry of Cement, 2007.
[17] N. Meller, C. Hall, A.C. Jupe, S.L. Colston, S.D.M. Jacques, P. Barnes, J. Phipps, The paste hydration of brownmillerite with and without gypsum: a time resolved synchrotron diffraction study at 30, 70, 100 and 150 °C, J Mat Chem 14 (2004) 428–435.
[18] M. Merlini, G. Artioli, T. Cerulli, F. Cella, A. Bravo, Tricalcium aluminate hydration in additivated systems. A crystallographic study by SR-XRPD, Cem Concr Res 38 (2008) 477–486.
[19] A.N. Christensen, N.V.Y. Scarlett, I.C. Madsen, T.R. Jensen, J.C. Hanson, Real time study of cement and clinker phases hydration, Dalton T (2003) 1529–1536.
[20] A.N. Christensen, T.R. Jensen, J.C. Hanson, Formation of ettringite, $Ca_6Al_2(SO_4)_3(OH)_{12}\cdot 26H_2O$, AFt, and monosulfate, $Ca_4Al_2O_6(SO_4)\cdot 14H_2O$, AFm-14, in hydrothermal hydration of Portland cement and of calcium aluminum oxide — calcium sulfate dihydrate mixtures studied by *in situ* synchrotron X-ray powder diffraction, J. Solid State Chem. 177 (2004) 1944–1951.
[21] A.C. Jupe, A.P. Wilkinson, K. Luke, G.P. Funkhouser, Slurry consistency and *in situ* synchrotron X-ray powder diffraction during the early hydration of Portland cements with calcium chloride, J. Am. Ceram. Soc. 90 (2007) 2595–2602.
[22] M. Merlini, G. Artioli, C. Meneghini, T. Cerulli, A. Bravo, F. Cella, The early hydration and the set of Portland cements: *in situ* X-ray powder diffraction studies, Powder Diffr. 22 (2007) 201–208.
[23] A.J.M. Cuberos, A.G. De la Torre, M.C. Martín-Sedeño, L. Moreno-Real, M. Merlini, L.M. Ordónez, M.A.G. Aranda, Phase development in conventional and active belite cement pastes by Rietveld analysis and chemical constraints, Cem. Concr. Res. 39 (2009) 833–842.
[24] M.C. Martin-Sedeño, A.J.M. Cuberos, A.G. De la Torre, G. Álvarez-Pinazo, L.M. Ordónez, M. Gateshki, M.A.G. Aranda, Aluminum-rich belite sulfoaluminate cements: clinkering and early age hydration, Cem. Concr. Res. 40 (2010) 359–369.
[25] L. Huizhen, Effect of structure and composition on reactivity of zeolite-tuff used as blending material of Portland cement, Proceedings of the 9th International Congress on the Chemistry of Cement, New Delhi, India, 1992, pp. 128–134.
[26] B.A. Fursenko, L.K. Kazantseva, I.A. Belitsky, Recent advances in the use of zeolitic tuffs in Russia for manufacturing building materials, in: C. Colella, F.A. Mumpton (Eds.), Natural Zeolites for the Third Millennium, De Frede Editore, Napoli, Italy, 2000, pp. 337–349.
[27] F. Canpolat, K. Yilmaz, M.M. Köse, M. Sümer, M.A. Yurdusev, Use of zeolite, coal bottom ash and fly ash as replacement materials in cement production, Cem. Concr. Res. 34 (2004) 731–735.
[28] N.-Q. Feng, G.-F. Peng, Applications of natural zeolite to construction and building materials in China, Constr. Build. Mater. 19 (2005) 579–584.
[29] R. Sersale, G. Frigione, Portland-zeolite-cement for minimizing alkali-aggregate expansion, Cem. Concr. Res. 17 (1987) 404–410.
[30] B. Uzal, L. Turanli, Studies on blended cements containing a high volume of natural pozzolans, Cem. Concr. Res. 33 (2003) 1777–1781.
[31] B. Yilmaz, A. Uçar, B. Öteyaka, V. Uz, Properties of zeolitic tuff (clinoptilolite) blended Portland cement, Build. Environ. 42 (2007) 3808–3815.
[32] A.A. Coelho, Topas Academic v4.1, 2007, http://www.members.optusnet.com.au/~alancoelho/.
[33] R.W. Cheary, A.A. Coelho, A fundamental parameters approach of X-ray line-profile fitting, J. Appl. Crystallogr. 25 (1992) 109–121.

[34] A.G. De la Torre, S. Bruque, J. Campo, M.A.G. Aranda, The superstructure of C_3S from synchrotron and neutron powder diffraction and its role in quantitative phase analyses, Cem. Concr. Res. 32 (2002) 1347–1356.
[35] W.G. Mumme, Crystal structure of tricalcium silicate from a Portland cement clinker and its application to quantitative XRD analysis, Neues Jahrb Mineral (1995) 145–160.
[36] W.G. Mumme, L. Cranswick, B. Chakoumakos, Rietveld crystal structure refinement from high temperature neutron powder diffraction data for the polymorphs of dicalcium silicate, Neues Jahrb Mineral 170 (1995) 171–188.
[37] P. Mondal, J.W. Jeffery, The crystal structure of tricalcium aluminate, $Ca_3Al_2O_6$, Acta Crystallogr. B31 (1975) 689–697.
[38] A.A. Colville, S. Geller, The crystal structure of brownmillerite, $CaFe_2AlO_5$, Acta Crystallogr. B27 (1971) 2311–2315.
[39] E. Hoehne, A more accurate determination of the crystal structure of anhydrite, $CaSO_4$, Kristallografiya 7 (1962) 690–700.
[40] B.F. Pedersen, D. Semmingsen, Neutron diffraction refinement of the structure of gypsum, $CaSO_4(H_2O)_2$, Acta Crystallogr. B38 (1982) 1074–1077.
[41] Y. Le Page, G. Donnay, Refinement of the crystal structure of low-quartz, Acta Crystallogr. B32 (1976) 2456–2459.
[42] W. Horst, T. Tagai, M. Korekawa, H. Jagodzinski, Modulated structure of a plagioclase An52: theory and structure determination, Z. Kristallogr. 157 (1981) 233–250.
[43] A. Alberti, E. Galli, G. Vezzalini, E. Passaglia, P.F. Zanazzi, Position of cations and water molecules in hydrated chabazite. Natural and Na-, Ca-, Sr-, and K-exchanged chabazites, Zeolites 2 (1982) 303–309.
[44] H.E. Petch, The hydrogen position in portlandite, $Ca(OH)_2$, as indicated by the electron distribution, Acta Crystallogr. 14 (1961) 950–957.
[45] F. Goetz-Neunhoeffer, J. Neubauer, Refined ettringite ($Ca_6Al_2(SO_4)_3(OH)_{12}.26H_2O$) structure for quantitative X-ray diffraction analysis, Powder Diffr. 21 (2006) 4–11.
[46] R. Allmann, Refinement of the hybrid layer structure, $(Ca_2Al(OH)_6)^+(0.5SO_4.3H_2O)^-$, Neues Jahrb Mineral (1977) 136–144.
[47] R.J. Hill, C.J. Howard, Quantitative phase analysis from neutron powder diffraction data using the Rietveld method, J. Appl. Crystallogr. 20 (1987) 467–474.
[48] R. Snellings, L. Machiels, G. Mertens, J. Elsen, Quantitative mineralogical analysis of zeolitised tuffaceous rocks using the Rietveld method, Geol Belg 13 (2010) 183–196.
[49] E.M. Gartner, J.F. Young, D.A. Damidot, I. Jawed, Hydration of Portland cement, in: J. Bensted, P. Barnes (Eds.), Structure and Performance of Cements, 2nd edition, Spon Press, London, 2002, pp. 57–113.
[50] J.C. Taylor, L.P. Aldridge, C.E. Matulis, I. Hinczak, X-ray powder diffraction analysis of cements, in: J. Bensted, P. Barnes (Eds.), Structure and Performance of Cements, 2nd edition, Spon Press, London, 2002, pp. 420–456.
[51] R. Kondo, K. Lee, M. Diamon, Kinetics and mechanisms of hydrothermal reaction in lime-quartz-water systems, J Ceram Soc (Japan) 84 (1976) 573–578.
[52] A.G. De la Torre, S. Bruque, M.A.G. Aranda, Rietveld quantitative amorphous content analysis, J. Appl. Crystallogr. 34 (2001) 196–202.
[53] I.G. Richardson, Tobermorite/jennite- and tobermorite/calcium hydroxide-based models for the structure of C–S–H: applicability to hardened pastes of tricalcium silicate, β-dicalcium silicate, Portland cement, and blends of Portland cement with blast-furnace slag, metakaolin, or silica fume, Cem. Concr. Res. 34 (2004) 1733–1777.
[54] F. Massazza, Pozzolana and pozzolanic cements, in: P.C. Hewlett (Ed.), Lea's Chemistry of Cement and Concrete, 4th edition, Butterworth-Heinemann, Oxford, UK, 2001, pp. 471–636.
[55] G. Renaudin, J. Russias, F. Leroux, F. Frizon, C. Cau-dit-Coumes, Structural characterization of C–S–H and C–A–S–H samples — part I: long-range order investigated by Rietveld analyses, J. Solid State Chem. 182 (2009) 3312–3319.
[56] D.L. Bish, J.M. Boak, Clinoptilolite–heulandite nomenclature, in: D.L. Bish, D.W. Ming (Eds.), Natural Zeolites: Occurrence, Properties, Applications, Reviews in Mineralogy and Geochemistry, Mineralogical Society of America, Washington D.C, 2001, pp. 207–216.
[57] M. Merlini, C. Meneghini, G. Artioli, T. Cerulli, Synchrotron radiation XRPD study on the early hydration of cements, Z Kristallogr Suppl 26 (2007) 411–416.
[58] J. Neubauer, F. Goetz-Neunhoeffer, U. Holland, D. Schmitt, P. Gaeberlein, M. Degenkolb, Crystal chemistry and microstructure of hydrated phases occurring during the early OPC hydration, Proceedings of the 12th International Congress on the Chemistry of Cement, 2007.
[59] G. Renaudin, Y. Filinchuk, J. Neubauer, F. Goetz-Neunhoeffer, A comparative structural study of wet and dried ettringite, Cem. Concr. Res. 40 (2010) 370–375.
[60] K. Garbev, G. Beuchle, M. Bornefeld, L. Black, P. Stemmermann, Cell dimensions and composition of nanocrystalline calcium silicate hydrate solid solutions. Part 1: synchrotron-based X-ray diffraction, J. Am. Ceram. Soc. 91 (2008) 3005–3014.